Appl. Phys. B 89, 573–577 (2007)
DOI: 10.1007/s00340-007-2831-3

Applied Physics B
Lasers and Optics

L. CHEN
G.P. WANG✉,*

Nanofocusing of light energy by ridged metal heterostructures

Key Laboratory of Acoustic and Photonic Materials and Devices, Ministry of Education and Department of Physics, Wuhan University, Wuhan 430072, P.R. China

Received: 9 September 2007 /
Revised version: 16 October 2007
Published online: 24 November 2007 • **© Springer-Verlag 2007**

ABSTRACT With regard to thin Ag and Al films of the same thickness, the phase velocity of surface plasmon polaritons (SPPs) on the Ag surface is smaller than that on the Al surface. We have designed a ridged metal heterostructure (RMH) for nanofocusing of light energy. Finite difference time domain simulations reveal that the RMHs constructed with both the Ag and Al films can result in giant local field enhancement, instead of around the sharp corners, as the triangular metal nanocrystals constructed with a homogeneous metal material do, in the middle part of the structures. Further assembly of the RMHs can construct interesting nanoantennas and array probes, implying potential applications of the RMHs in nanophotonics and biophotonics.

PACS 42.82.Et; 82.79.Pw; 85.60.Gz

1 Introduction

Efficient energy interconversion between propagation light and the localized field of light is important for highly-sensitive biological and chemical detectors. Surface enhanced Raman scattering (SERS) for probing single molecules is one of many typical examples [1–3]. So far, several nanostructures such as sharp metallic tips [4, 6] and "bowtie" antennas [7–10] etc. have been proposed for these purposes. It was demonstrated that the local optical intensity close to a sharp Au tip can be enhanced to 1000 times higher than that of the incident light [5], while the intensity enhancement produced by the "bowtie" antennas at the so-called "hot spot" is in excess of 1500 [9]. By using two different metal materials, the authors have proposed and demonstrated a series of metal heterowaveguides for nanofocusing, nanoguiding, and the directional beaming of light, as well as for use as Bragg reflectors [11–15].

In this paper, we will demonstrate ridged metal heterostructures (RMHs) for giant nanofocusing of light energy and local field enhancement. The RMHs are constructed by sandwiching a triangular Ag ridge into two Al ones. Although some triangular metal nanocrystals constructed with a homogeneous metal material have recently been synthesized for the purpose of local enhancement [16–18], the lack of controllable fabrication and the localization of strong local field intensity around the corners of these structures [18], are not convenient in some cases for realistic applications. In contrast, finite difference time domain (FDTD) simulations demonstrate that the proposed RMHs in this article can not only produce giant local field intensity in the nanoscale domain, but can also confine light energy in the centric part of the structures.

2 Principle of RMHs for nanofocusing

Considering a two-dimensional (2D) air-metal-air system as shown in the inset of Fig. 1a, where d is the thickness of metal film, ε_1 and ε_m represent the relative permittivities of air and metal material, respectively, we can write the amplitude distribution of electric field E_z of surface plasmon polariton (SPP) modes in the interfaces of metal and air as:

$$E_z = \begin{cases} A\mathrm{e}^{-px}, & 0 \le x < \infty \\ B\mathrm{e}^{-kx} + Ce^{kx}, & -d \le x \le 0 \\ D\mathrm{e}^{px}, & -\infty < x \le -d \end{cases}, \tag{1}$$

where $k = (\beta^2 - k_0^2\varepsilon_1)^{1/2}$ and $p = (\beta^2 - k_0^2\varepsilon_\mathrm{m})^{1/2}$ are the transverse propagation constants (along the x-axis) of SPPs in dielectric (ε_1) and metal (ε_m), respectively, β is the propagation constant of SPPs along the z direction, k_0 is the wavenumber of incident light in vacuum, and A, B, C, and D are the mode amplitudes of SPPs in the metal and dielectric, respectively. A similar magnetic field distribution H_y can be obtained by applying Maxwell's equations to (1). By employing the boundary condition that E_z and H_y must be continuous in the interfaces and solving the E_z and H_y equations, we can get the dispersion relation of SPPs in the system as [19]:

$$kd = \ln\left|\frac{1 - \frac{p\varepsilon_\mathrm{m}}{k\varepsilon_1}}{1 + \frac{p\varepsilon_\mathrm{m}}{k\varepsilon_1}}\right|. \tag{2}$$

For a certain thickness d of metal film, one can get the propagation constant β of SPPs from (2) [19]. Then we can

✉ Fax: +86-27-87342531, E-mail: kp_wang@hotmail.com
Present address: Key Laboratory of Acoustic and Photonic Materials and Devices, Ministry of Education and Department of Physics, Wuhan University, Wuhan 430072, P.R. China

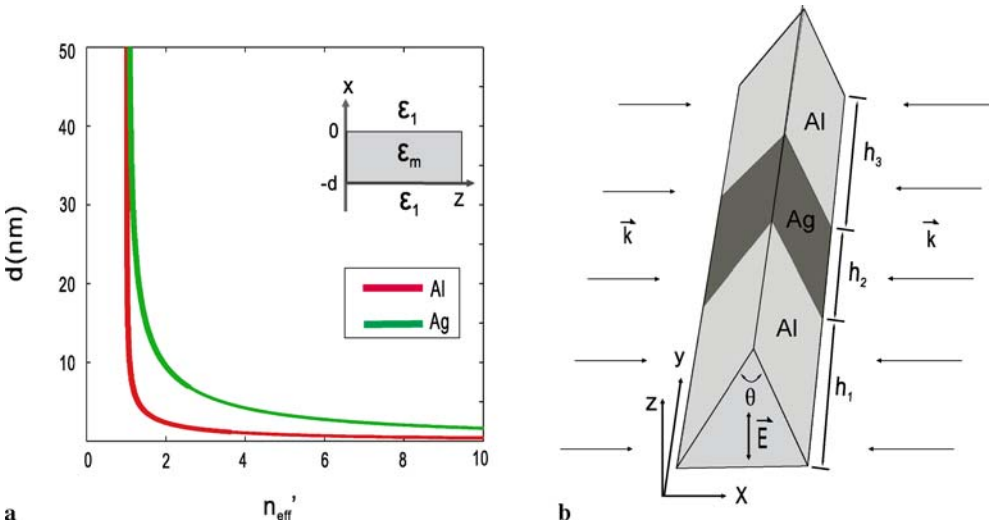

FIGURE 1 (**a**) Dependence of the real part of effective refraction index n'_{eff} of SPPs on the thicknesses d of metals Ag and Al films, respectively. *Inset*, scheme of the 2D air-metal-air system. (**b**) Scheme of the designed RMHs constructed by sandwiching a triangular Ag ridge into two Al ones. h_1, h_3, h_2, and θ denote the lengths of Al and Ag ridges and the vertex angle of the RMHs, respectively. The whole height of the RMHs in the z direction is 375 nm

define the effective refraction index n_{eff} ($n_{\text{eff}} = n'_{\text{eff}} + jn''_{\text{eff}}$) of SPPs on the interface between the air and metal as:

$$n_{\text{eff}} = n'_{\text{eff}} + jn''_{\text{eff}} = \frac{\beta}{k_0}\,, \tag{3}$$

where n'_{eff} and n''_{eff} represent the real and imaginary parts of the effective refraction index, respectively. The phase velocity υ_{p} of SPPs is determined by $\upsilon_{\text{p}} = c/n'_{\text{eff}}$, where c is the velocity of light in vacuum.

Figure 1a shows the dependence of n'_{eff} on the thickness d of the Ag and Al films, respectively. In the calculations, the wavelength of the exciting light $\lambda = 539.1$ nm and the dielectric constants $\varepsilon_{\text{m1}} = -10.55 + j0.84$ and $\varepsilon_{\text{m2}} = -42.13 + j11.96$ of Ag and Al at this wavelength [20] are used, respectively. From the figure, one can see that, with the same thickness d, n'_{eff} of SPPs on the Ag surface is always greater than that on the Al surface, and the difference of n'_{eff} becomes greater as d reduces in a certain range. Furthermore, n'_{eff} decreases and asymptotically tends to be infinite as d is approaching zero for each case. From conventional waveguide optics, we know that electromagnetic waves tend to propagate in the medium with higher refractive index than its adjacent ones, or in other words, electromagnetic waves prefer to travel with lower phase velocity [21]. With this in mind, we designed a type of RMHs, as is schematically shown in Fig. 1b, for focusing light energy into the nanoscale domain, where a triangular Ag ridge is sandwiched by two Al ridges. The cross section of the ridges is an isosceles triangle. Geometric parameters of the structure such as the height (along z direction, 375 nm, fixed), the vertex angle θ, and the lengths h_1, h_3, and h_2 of metals Al and Ag are shown in the figure. In our FDTD simulations, the spatial and temporal steps are set at $\Delta x = \Delta y = \Delta z = 5$ nm and $\Delta t = x/2c$, respectively, and the first-order Mur absorbing boundary conditions are used at the boundaries of the computational window [22].

In order to get a symmetrical electric field distribution, we assume two plane waves (in the y–z plane) with unity amplitude to symmetrically illuminate the structures from both sides of the RMHs (Fig. 1b). The wave vector $\boldsymbol{k}$ and electric field vector $\boldsymbol{E}$ are set in the x and z directions, respectively. To quantitatively estimate the enhancement effect of the RMHs on the local electric field, we define the normalized electric field intensity $|E|^2 = |E_2|^2/|E_1|^2$ to represent the field distributions in all the situations, where $|E_1|^2$ and $|E_2|^2$ represent the steady-state electric field intensities of both without and with RMHs, respectively.

3 Nanofocusing properties of RMHs

Figure 2a and b shows the calculated gray distributions of $|E|^2$ at the middle part of the RMH in x–z plane and along the y axis as the RMH is with $h_1 = h_3 = 250$ nm, $h_2 = 65$ nm, and vertex angle $\theta = 30°$, respectively. From the figure, we can see that not only the electric field is tightly confined around the ridge of the RMH (Fig. 2a), but is mainly localized in the part of Ag ridge (Fig. 2b). Figure 2c shows the corresponding profile of the $|E|^2$ distribution along the y direction (parallel to the ridge of the RMH). It can be seen that the normalized electric field intensity reaches about 1200 at the middle part of the RMH, while in the side parts (Al ridges), a much weaker electric field intensity appears.

When the Al parts in the above RMH are removed, the structure consists of Ag only and is similar to the conventional triangular metal nanocrystals [16–18]. Figure 2d–f shows the calculated electric field intensity $|E|^2$ at the middle part of the Ag ridge in x–z plane, along the y axis, and the corresponding profile of $|E|^2$ along the y direction of the structure, respectively, where the geometric parameters of the Ag ridge (375 nm high and 65 nm long) and illuminating conditions are the same as that of Fig. 2a–c. As it is expected that, though as strong as about 1240 normalized electric field intensity can be reached, the giant local electric field is localized around both tips of the Ag ridge, while at its middle part, only about a 90 normalized electric field intensity is observed (Fig. 2e and f), which is similar to the cases of homogeneous metal nanocrystals produced [18].

Making the electric field vector $\boldsymbol{E}$ of illuminating light perpendicular to the z direction but keeping other geometric parameters fixed, the calculated result reveals that the normalized electric field intensity shows no enhancement effect. This suggests that it is crucial to make the polarization direction of the illuminating light perpendicular to the ridge of

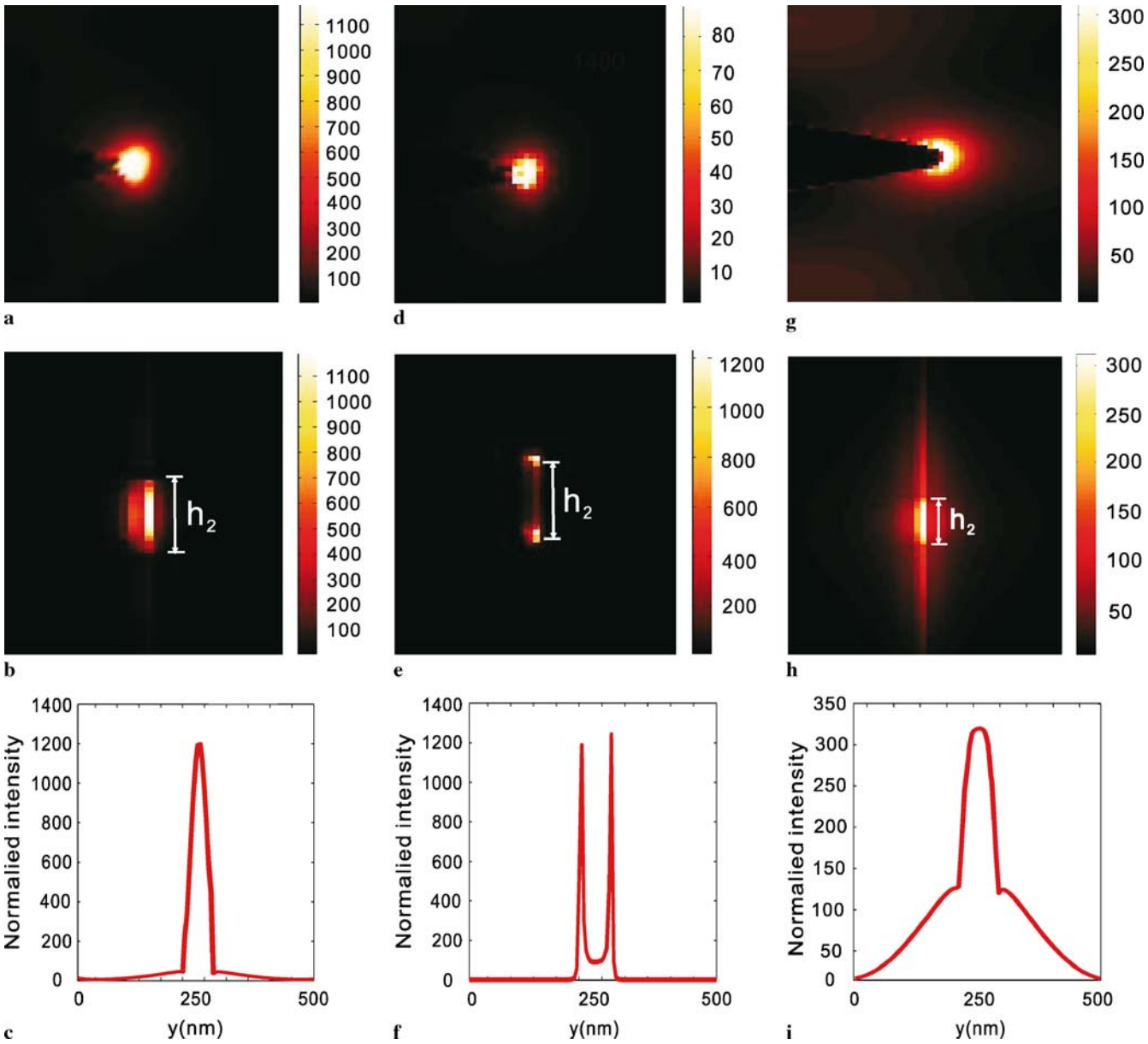

FIGURE 2 Calculated gray distributions of $|E|^2$ at the middle part in x–z plane [(**a**), (**d**), (**g**)], along the y axis [(**b**), (**e**), (**h**)], and $|E|^2$ profiles along the y direction [(**c**), (**f**), (**i**)] for the RMHs with [(**a**)–(**c**), (**g**)–(**i**)] and without Al ridges [(**d**)–(**f**)], respectively. In the calculations, $h_1 = h_3 = 250$ nm, $h_2 = 65$ nm, and $\theta = 30°$ are used. In (**a**)–(**f**), the structures are with a sharp tip while in (**g**)–(**i**) the RMH is with a round tip with a 15 nm radius

RMHs (along the z axis) for obtaining an enhanced local electric field [4, 5].

The physics behind the giant enhancement effect of the RMHs can be attributed to following reasons: firstly, when the polarization direction of the incident light is perpendicular to the ridge direction (z axis), there is a large surface charge accumulation on the ridge, which will induce a giant local field intensity in the vicinity of the ridge [4, 5]. Secondly, as is well known, electromagnetic waves tend to propagate with lower phase velocity [21]. From Fig. 1a we see that the phase velocity of SPPs on the Ag surface is always smaller than that on the Al surface. Therefore, SPPs will concentrate into the Ag region of the RMHs. Furthermore, because n'_{eff} reduces and asymptotically tends to be infinite as the thickness d of the Ag film is approaching zero, the phase velocity of SPPs on the surface of the Ag film tends to zero, which leads to the slowdown and asymptotically stop of SPPs at the vertex of the ridge. As a result, the accumulation of SPPs on the ridge of the Ag region occurs.

Figure 3a shows the dependence of the normalized electric field intensity $|E|^2$ at the middle part of the RMHs on the length h_2 of Ag ridge, while $h_1 = h_3 = 250$ nm and $\theta = 30°$ are fixed. It can be seen that, as $h_2 < 95$ nm, the field intensity shows a rapid increase with h_2. While as h_2 is larger than 95 nm, it falls gradually as h_2 is increased. When $h_2 = 95$ nm, a maximum electric field intensity of about 1400 appears. This means that, to achieve strongest electric field intensity, an optimal h_2 is required. Figure 3b presents the dependence of $|E|^2$ on the vertex angle θ of RMHs with $h_1 = h_3 = 250$ nm and $h_2 = 65$ nm, respectively. From the figure, one sees that the

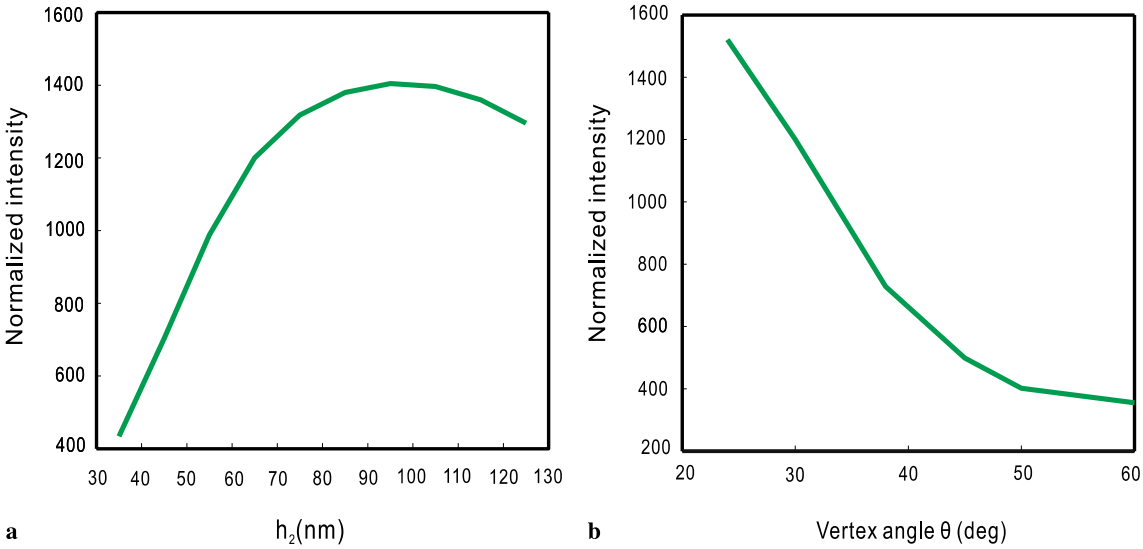

FIGURE 3 Dependence of the normalized electric field intensity on (**a**) the length h_2 of Ag ridge ($h_1 = h_3 = 250$ nm and $\theta = 30°$) and (**b**) the vertex angle θ($h_1 = h_3 = 250$ nm and $h_2 = 65$ nm)

electric field intensity increases monotonously with the decrease of the vertex angle θ. For instance, as the vertex angle θ equals 24° , as high as 1480 normalized electric field intensity in the middle part of the RMH can be obtained (Fig. 3b). This is due to the enhancement of charge density and slowdown of SPPs propagation on the ridge of RMHs as the vertex angle θ is decreased. From above discussions, we can see that by combining the optimization of both the length of Ag ridge and vertex angle θ of RMHs simultaneously, much stronger local electric field can be realized.

However, realization of the sharp features is limited in actual situation, which in turn may reduce the field enhancement of RMHs. Figure 2g–i shown are the calculated electric field intensity $|E|^2$ at the middle part in x–z plane, along y axis, and the corresponding profile of $|E|^2$ along y direction of a RMH, respectively, as the RMH is with a round tip with 15 nm radius while all the other condition are the same as that of Fig. 2a–c. It can be seen that the normalized electric field decreases from 1200 (Fig. 2c) to about 315 (Fig. 2i). As the tip radius is set at 10 nm, 20 nm, and 25 nm, respectively, the normalized electric intensity changes to 380, 280, and 250, respectively, meaning that the electric intensity is decreased with enlarged tip radius. This can be attributed to the reduction of charge density and less accumulation of SPPs at the tip as the tip radius is increased.

4 RMHs for nanoantennas and array probes

Figure 4a illustrates the normalized light distribution at the middle of h_2 (x–z plane) of a nanoscale antenna consisting of two RMHs with 20 nm gap (see the inset of the figure), of which all the parameters are the same as that of Fig. 2a–c. The highest normalized field intensity is as high as 1605 and the light spot is confined in a spot of size 5 nm × 20 nm in the x–z plane. Figure 4b schematically shows a pair of RMHs for multiple nanofocusing, where h_1, h_2, and h_3 are set at 200 nm, 65 nm, and 250 nm, respectively. Figure 4c presents the normalized light field distribution on a plane (x–y

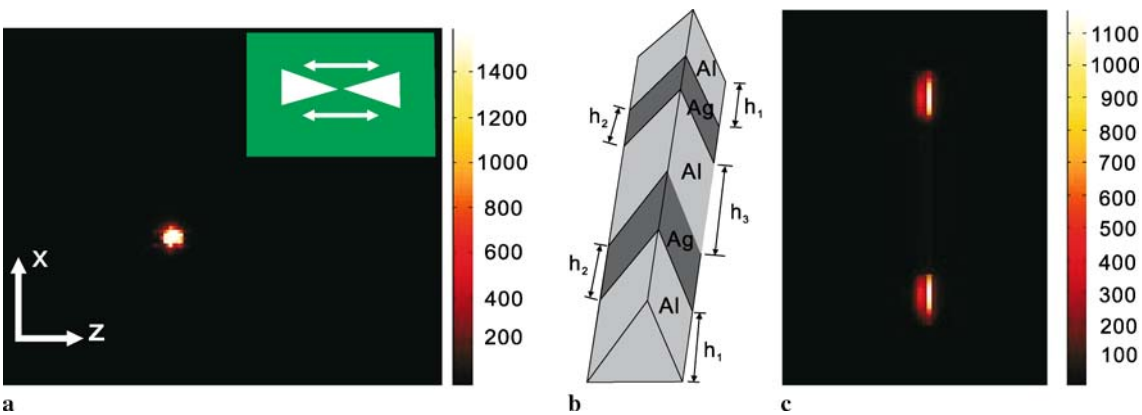

FIGURE 4 (**a**) Normalized light distribution at the middle part of a nanoscale antenna consisting of two RMHs with a 20 nm gap. *Inset*, scheme of the antenna. (**b**) Scheme of a pair of RMHs for multiple nanofocusing. (**c**) Normalized electric field intensity distribution on a plane (x–y plane) 5 nm away from the top of the pairs of RMHs as $h_1 = 200$ nm, $h_2 = 65$ nm and $h_3 = 250$ nm. In the calculations, if without notation, other geometrical parameters and illumination condition are the same as that of Fig. 2a–c

plane) 5 nm away from the top of the RMHs. In the calculation, other parameters and illumination conditions are the same as that of Fig. 2a–c. One can see that two enhanced optical spots (with the same normalized light intensity as that of Fig. 2b) are localized at Ag regions of the RMHs. By extending the RMHs in the z direction and the x–y plane, we can construct one- and two-dimensional RMH arrays for multiple nanofocusing, which is beneficial for array sensing.

It should be noted that the welding of two nanosized materials may result in the formation of a blur boundary due to the inter-diffusion or boundary stress, which may limit the final geometry of the structures. By carefully controlling and optimizing the fabrication techniques of the metal heterostructures, it is possible to get a sharper boundary between two different metals [23].

5 Conclusions

In conclusion, we have designed and demonstrated a type of RMH for focusing light energy into the nanoscale domain. Instead of localizing the strong electric field around the sharp corners of the nanostructures as metal tips and homogeneous metal nanocrystals do, the RMHs can enhance the local electric field in the middle part of the structures. Further enhancement by RMHs constructed nanoantennas and array nanofocusing by multiple RMHs, imply various convenient applications of the RMHs in nanophotonics and biophotonics, such as high-density optical data storage, near-field optical microscopy, optical nanolithography, and bio- and chemosensing etc.

ACKNOWLEDGEMENTS We would like to thank Dr. Z.Y. Li for fruitful discussions. This work is supported by the National Basic Research Program of China (grant 2006CB302900, 2007CB935304), the National Natural Science Foundation of China (Grant 60736041, 10774116, 10574101), and the program of NCET (Grant 04-0678).

REFERENCES

1 S. Nie, S.R. Emory, Science **275**, 1102 (1997)
2 K. Kneipp, Y. Wang, H. Kneipp, L.T. Perelman, I. Itzkan, R. Dasari, M.S. Feld, Phys. Rev. Lett. **78**, 1667 (1997)
3 K. Kneipp, H. Kneipp, I. Itzkan, R.R. Dasari, M.S. Feld, J. Phys. Condens. Matter **14**, R597 (2002)
4 L. Novotny, R.X. Bian, X.S. Xie, Phys. Rev. Lett. **79**, 645 (1997)
5 E.J. Sanchez, L. Novotny, X.S. Xie, Phys. Rev. Lett. **82**, 4014 (1999)
6 M.I. Stockman, Phys. Rev. Lett. **93**, 137 404 (2004)
7 D.P. Fromm, A. Sundaramurthy, P.J. Schuck, G. Kino, W.E. Moerner, Nano Lett. **4**, 957 (2004)
8 P. Muhlschlegel, H.J. Eisler, O.J.F. Martin, B. Hecht, D.W. Pohl, Science **308**, 1607 (2005)
9 P.J. Schuck, D.P. Fromm, A. Sundaramurthy, G.S. Kino, W.E. Moerner, Phys. Rev. Lett. **94**, 017 402 (2005)
10 E. Cubukcu, E.A. Kort, K.B. Crozier, F. Capasso, Appl. Phys. Lett. **89**, 093 120 (2006)
11 B. Wang, G.P. Wang, Appl. Phys. Lett. **85**, 3599 (2004)
12 B. Wang, G.P. Wang, Appl. Phys. Lett. **88**, 013 114 (2006)
13 B. Wang, G.P. Wang, Appl. Phys. Lett. **87**, 013 107 (2005)
14 G.P. Wang, B. Wang, J. Opt. Soc. Am. B **23**, 1660 (2006)
15 L. Chen, B. Wang, G.P. Wang, Appl. Phys. Lett. **89**, 243 120 (2006)
16 R.C. Jin, Y.W. Cao, C.A. Mirkin, K.L. Kelly, G.C. Schatz, J.G. Zheng, Science **294**, 1901 (2001)
17 R.C. Jin, Y.C. Cao, E. Hao, G.S.M. Traux, G.C. Schatz, C.A. Mirkin, Nature **425**, 487 (2003)
18 E. Hao, R.C. Bailey, G.C. Schatz, J.T. Hupp, S. Li, Nano Lett. **4**, 327 (2004)
19 E.N. Economow, Phys. Rev. B **182**, 539 (1969)
20 E.D. Palik, *Handbook of Optical Constants of Solids* (Academic, New York, 1985), pp. 356 and 405, Chapt. 11
21 P.K. Tien, Phys. Rev. Mod. **49**, 361 (1977)
22 G. Mur, IEEE Trans. Electromagn. Compat. **40**, 100 (1998)
23 K. Tazuko, M. Shintaro, M. Yoshiteru, K. Kunio, T. Akira, Chin. Phys. Lett. **24**, 2827 (2007)